Chapter 9
Nickel-Based Superalloys

D.V.V. Satyanarayana and N. Eswara Prasad

Abstract Nickel-based superalloys are an exceptional class of structural materials for high temperature applications, particularly in the challenging environment of the turbine sections of aircraft engines. Continued improvements in the properties of these materials have been possible through close control of chemistry and microstructure as well as the introduction of advanced processing technologies. Surface modification by application of coating technology concurrent with the introduction of directional structures and then single crystals, has extended the useful temperature range of superalloys. Further improvements are likely with the development and implementation of tools for alloy design, microstructure-process evolution, and mechanical-property modelling. To date, six generations of single crystal (SC) nickel-based superalloys have been developed with improved creep properties and phase stability. Therefore it appears that the evolution of advanced nickel-based superalloys is a never ending process, and their replacement in turbine engine applications seems to be impossible at least for a few more decades. The present chapter is a brief review of various aspects pertaining to chemical composition, heat treatment, microstructure, properties and applications of both cast, and wrought alloys as well as the evolution of advanced cast nickel-based superalloys.

D.V.V. Satyanarayana (✉)
DMRL, Hyderabad, India
e-mail: dvvsn@rediffmail.com; dvvsnarayana@dmrl.drdo.in; dvvsn25@gmail.com

N. Eswara Prasad
DMSRDE, DRDO, Kanpur, India
e-mail: nep@dmsrde.drdo.in; neswarap@rediffmail.com

9.1 Introduction

"Superalloys" belong to a group of alloys developed after World War II for use in turbo-superchargers and aircraft gas turbine engines that required high performance at elevated temperatures. The use of these alloys has subsequently expanded too many other areas, including land-based gas turbines, rocket engines, chemical, and petroleum plants. These materials are particularly well suited for these demanding applications because of their ability to retain most of their strength even after long exposure times above 650 °C. Their versatility stems from the fact that they combine high strength with good low-temperature ductility and excellent surface stability. Several books [1–5] as well as numerous papers and reports [6–26] giving detailed account of various aspects of superalloys are already available in the open literature. Nevertheless, an attempt has been made in the chapter of this book is not only to briefly present the physical metallurgical aspects and mechanical properties of nickel-based superalloys, but also include details on the evolution of advanced cast nickel-based superalloys so as to prepare a brief up-to-date compilation of information on this class of alloys. Indian efforts in producing type-certified superalloy primary and secondary products as well as select components are surveyed in Chap. 24 in Volume 2 of these Source Books.

9.2 Classification of Nickel-Based Superalloys

Superalloys are the major materials used for the turbine sections of aircraft. Nickel-based superalloys along with iron-based/ iron-nickel-based and cobalt-based superalloys are used in wrought, cast, powder metallurgy, and cast-single crystal forms to meet the demands imposed by efficient high-temperature use. Figure 9.1 illustrates the use of nickel-based superalloys and other alloys for various sections

Fig. 9.1 Sectional view of an advanced aircraft gas turbine engine (*Source* Michael Cervenka, Rolls-Royce) [5]
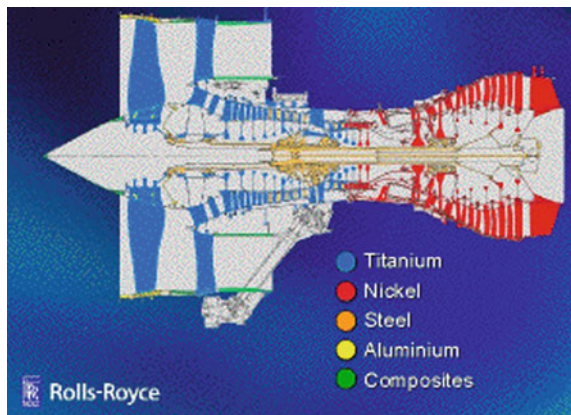
of an aircraft gas turbine engine, where it is seen that superalloys are employed in the combustion chamber and turbine sections.

The superalloys are based on Group VIII B elements of the Periodic Table, and usually consist of various combinations of Fe, Ni, Co, and Cr, as well as lesser amounts of W, Mo, Ta, Nb, Ti, and Al. The three major classes of superalloys are nickel-, iron-/iron-nickel-, and cobalt-based alloys. In all cases, the crystal structure is face centered cubic (fcc) at all temperatures, owing to stabilization of this structure by the alloying elements, particularly nickel. A large number of superalloys have been invented and studied, and many have been patented. However, only a few are extensively used. The present chapter considers only nickel-based superalloys.

All superalloys products can be classified into three main categories [3–5]: (i) cast, (ii) wrought, and (3) powder metallurgy (PM). Examples of alloys in these categories are listed in Tables 9.1 and 9.2. Wrought alloys are generally more homogeneous with more uniform microstructures than cast alloys, which usually have segregation caused by the solidification process. As a consequence, wrought alloys are considered more ductile and exhibit more consistent mechanical properties.

Early in the history of superalloys, the development of new alloy compositions was successful only if melt processing techniques were advanced enough to produce commercial-size quantities. As higher strength and more highly alloyed materials were produced, melt processes were developed which reduced ingot

Table 9.1 Chemical compositions of wrought nickel-based superalloys

Alloy	Cr	Al	Co	Mo	W	Nb	Ti	B	Fe	C	Others	Ni
Combustor applications												
Hastelloy X	22	–	1.5	9	0.7	–	–	0.005	1.9	0.07	–	Bal
Nimonic C-263	20	0.4	20	6	–	–	2.1	–	0.4	0.06	–	Bal
IN617	22	1.2	12.5	8.5	–	–	–	–	–	0.05	–	Bal
IN 230	22	0.35	5	2	14	–	–	0.015	3	0.1	–	Bal
Disc applications (aircraft engines and industrial gas turbines)												
IN 706	16	–	–	–	–	2.9	1.8	–	37	0.03	–	Bal
IN 718	19	0.5	–	3	–	5.1	0.9	–	18.5	0.03	–	Bal
Udimet 720	18	2.5	14.8	3	1.25	–	5	0.033	–	0.035	0.03 Zr	Bal
Udimet 720 LI	16	2.5	15	3	1.25	–	5	0.018	–	0.025	0.03 Zr	Bal
IN 100[a]	10	5.5	15	3	–	–	4.7	0.015	–	0.15	0.06 Zr; 1 V	Bal
Rene 88 DT[a]	16	2.1	13	4	4	0.7	3.7	0.015	–	0.03	0.03 Zr	Bal

[a]Processed by powder metallurgy(PM) route

Table 9.2 Chemical compositions of cast nickel-based superalloys

Alloy	Cr	Al	Co	Mo	W	Nb	Ti	B	Fe	C	Others	Ni
IN 713	12.5	6.1	–	4.2	–	2	0.8	0.01	–	0.12	0.1 Zr	Bal.
IN 100	10	5.5	15	3	–	–	4.7	0.01	–	0.18	0.06 Zr	Bal.
Mar-M200	9	5.5	15	–	12.5	1.8	2	0.015	–	0.14	0.05 Zr	Bal.
Mar-M246	9	5.5	10	2.5	10	–	1.5	0.015	–	0.14	0.05 Zr; 1.5 Ta	Bal.
Mar-M246 +Hf	8	5.5	10	2.5	10	–	1.5	0.015	–	0.15	0.05 Zr; 1.5 Ta, 1.5 Hf	Bal.
Rene 80 + Hf	14	3	9.5	4	4	–	4.7	0.015	–	0.15	0.01 Zr; 0.8 Hf	Bal.
IN 738	16	3.4	8.5	1.75	2.6	0.9	3.4	0.01	–	0.11	0.04 Zr; 1.75 Ta	Bal.

segregation and allowed sufficient ingot sizes such that subsequent thermome-chanical processing was adequate to homogenize the macrostructures and microstructures.

The development of PM superalloys arose when conventional melt processing methods were inadequate for highly alloyed compositions. Ingots cast from these advanced compositions would either self-destruct due to thermal stress, or show severe dendritic segregation, which would be impractical to homogenize.

9.3 Physical Metallurgy

9.3.1 Chemical Composition

Nickel-based alloys can be either solid solution or precipitation strengthened. Solid solution strengthened alloys, such as Hastelloy X, are used in applications requiring only modest strength, e.g., combustion chamber walls. For the most demanding applications, such as high pressure turbine blades and vanes, precipitation strengthened alloys are required.

Most nickel-based alloys contain 10–20 % Cr, up to 8 % Al and Ti, 5–10 % Co, and small amounts of B, Zr, and C. Other common additions are Mo, W, Ta, Hf, and Nb. The elemental additions in Ni-based superalloys can be categorized as (i) γ formers (elements that tend to partition to the matrix), i.e. solid solution strength-eners, (ii) γ′ formers (elements that partition to the γ′ precipitate), (iii) carbide formers, and (iv) finally, the elements that segregate to the grain boundaries. The roles of alloying elements in the formation of various phases are described in Table 9.3 as well as in Fig. 9.2.

Elements which are considered γ formers are Group V, VI, and VII elements of the Periodic Table such as Co, Cr, Mo, W, and Fe. γ′ formers come from group III,

Table 9.3 Alloying elements in nickel-based superalloys and their role

Elements	Effects
Ni	Stabilizes fcc matrix, forms γ' (Ni_3(Al,Ti)), and inhibits formation of deleterious phases
Cr	Imparts oxidation and sulphidation resistance as well as solid solution strengthening, and forms grain boundary carbides
Co	Raises solvus temperature of γ' and lowers stacking fault energy (thereby making cross-slip of screw dislocations more difficult)
Mo, Ta and W	solid solution strengthening and formation of MC-type carbides
Ti	Forms γ' (Ni_3(Al,Ti)) and MC-type carbides
Al	Forms γ' (Ni_3(Al,Ti)) and improves oxidation resistance
B and Zr	Improve stress rupture properties and retard grain boundary Ni_3Ti formation
La and Y	Improve oxidation resistance
C	Formation of carbides (MC, $M_{23}C_6$ etc., type)
Nb and Ta	Form γ'' (Ni_3Nb) and MC-type carbides

IV, and V elements and include Al, Ti, Nb, Ta, Hf. Furthermore, Co, Fe, Cr, Nb, Ta, Mo, W, V, Ti, and Al are solid solution strengtheners in both γ and γ'. There are, therefore, limits to the concentrations of these elements that can be added without inducing precipitation.

It is particularly important to avoid certain embrittling phases such as Laves and Sigma. There are no simple rules governing the critical concentrations. A major concern in the design of new alloys, and in defining specification limits for the acceptable range of individual alloying elements, is the avoidance of a class of phases known as topologically closed packed phases (TCPs). These phases are typically rich in refractory alloying elements and possess complex crystal structures characterized by closed-packed layers of atoms (atomic coordination number >12).

Examples of TCPs include the orthorhombic P phase, the tetragonal σ phase, and the rhombohedral R and μ phases [27–31]. TCP phases are detrimental because they not only deplete strengthening elements from the microstructure but also serve as crack-initiation sites during cyclic loading [4, 27–29]. However, precipitation kinetics for these phases is often very sluggish, resulting in precipitation only after extended times in service.

The main carbide formers are C, Cr, Mo, W, C, Nb, Ta, Ti, and Hf. The carbides tend to precipitate at grain boundaries and hence reduce the tendency for grain boundary sliding, thereby improving the creep resistance. Also, polycrystalline superalloys contain grain boundary strengthening elements such as boron and zirconium (and also carbon, already mentioned above). The resulting increase in grain boundary cohesive strength improves creep rupture strength and ductility.

Chromium and aluminium are essential for oxidation resistance, and small quantities of yttrium help the service-induced oxide scale to cohere to the substrate.

New alloy design tools based on the Calphad method [32–35] are increasingly used in the design of new alloys and to establish or modify specification ranges for
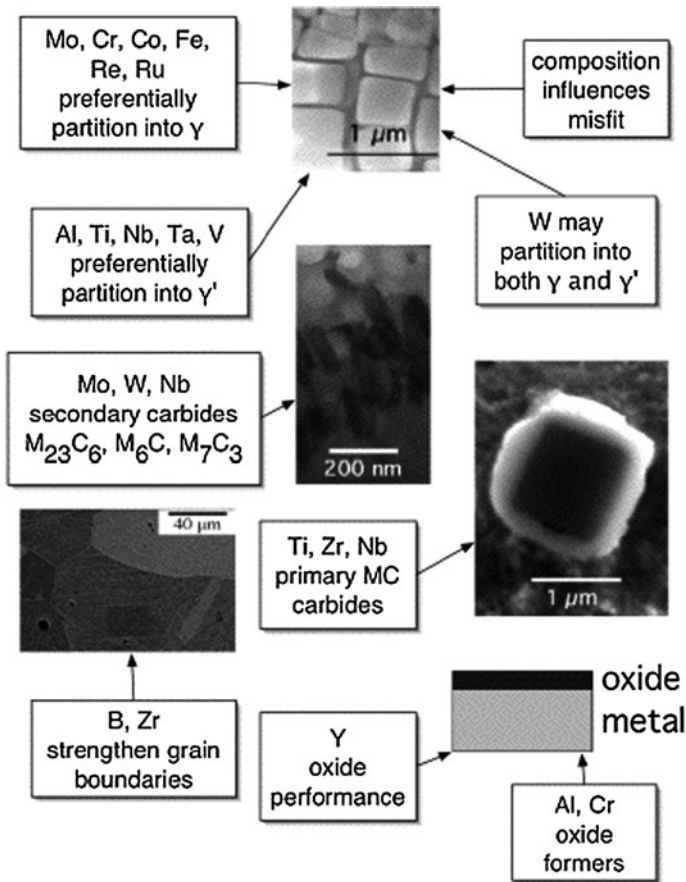
Fig. 9.2 Role of alloying elements in nickel-based superalloys

existing alloys to avoid deleterious phases. The ability to predict phase compositions and their ranges of stability depends on the development of thermodynamic models for the complex intermetallic phases and on the availability of databases to validate the modelling.

9.3.2 Microstructural Constituents

The major phases present in most nickel-based superalloys are as follows [1–5, 11, 12]:

Gamma (γ): The continuous matrix (called gamma) is an fcc nickel-based austenitic phase that usually contains a high percentage of solid solution elements such as Co, Cr, Mo, and W.

Gamma Prime (γ'): The primary strengthening phase in nickel-based superalloys is $Ni_3(Al,Ti)$, and is called gamma prime (γ'). Aluminium and titanium are the major alloying elements in γ', and are added in amounts and mutual proportions to precipitate a high volume fraction of γ' in the matrix. In some modern alloys the volume fraction of γ' is around 70 %.

γ' is a coherently precipitating phase (i.e. the crystal planes of the precipitate are in registry with the gamma matrix) with an ordered L12 (fcc) crystal structure. The close match in matrix/precipitate lattice parameter ($\sim$ 0–1 %) combined with the chemical compatibility allows γ' to precipitate homogeneously throughout the matrix and have long-time stability. In addition, γ' is quite ductile and thus imparts strength to the matrix without lowering the fracture toughness of the alloy.

There are many factors that contribute to the hardening imparted by the γ' and include γ' fault energy, γ' strength, coherency strains, volume fraction of γ', and γ' particle size.

Extremely small γ' precipitates always occur as spheres, owing to the dominance of minimizing the surface energy. For larger coherent precipitates it becomes more important to minimize the interfacial energy, and this result in γ' forming cubes, thereby allowing the crystallographic planes of the cubic matrix and precipitate to remain continuous. Thus as the γ' volume fraction increases, the morphology changes from spheres to cubes, or plates. However, coherency can be lost by overageing, and this is evidenced by directional coarsening (change in aspect ratio) and rounding of the cube edges.

Carbides: Carbon, added at levels of 0.05–0.2 %, combines with reactive and refractory elements such as titanium, tantalum, and hafnium to form carbides (e.g. TiC, TaC, or HfC). During heat treatment and service, these begin to decompose and form lower carbides such as $M_{23}C_6$ and M_6C, which tend to form on the grain boundaries [3, 4, 12]. These common carbides all have an fcc crystal structure. In general, carbides are considered to be beneficial by increasing the creep rupture strength at high temperatures.

TCP phases: These are generally undesirable brittle phases that can form during heat treatment or service. TCPs (σ, μ, Laves, etc.) usually form as plates (which appear as needles in 2-D micrographs). The plate-like structure adversely affects the ductility and creep rupture strength. Sigma appears to be the most deleterious, while strength retention has been observed in some alloys containing μ and Lave phases.

TCPs are potentially damaging for two main reasons: they sequester γ and γ' strengthening elements in a non-useful form, thus reducing the overall creep strength, and they can act as crack initiators because of their brittle nature [3, 4, 11, 12].

9.3.3 Heat Treatment

To optimize properties (often of an alloy/coating system), solution-treated nickel-based superalloys are aged at two different temperatures within the γ/γ'

phase field. The higher temperature heat treatment precipitates coarser particles of
γ'. The lower temperature heat treatment leads to a finer, secondary dispersion of γ'.
The net result is a bimodal distribution of γ'. Typical microstructures of wrought
and cast nickel-based superalloys are illustrated in Figs. 9.3, 9.4 and 9.5.

The solution heat treatment temperature determines not only the amount of γ'
that dissolves, but also the γ grain size. This coarsens if all the γ' is dissolved, since
the grain boundaries are no longer pinned by precipitates. Typical heat treatment
cycles (combinations of solution and ageing treatments) for wrought and cast
superalloys are given in Table 9.4.

Fig. 9.3 Wrought alloy microstructures: **a** equiaxed annealed grain structure, **b** coarse MC-type (TiC) carbides within grains and $M_{23}C_6$-type ($Cr_{23}C_6$) carbides along grain boundaries, and **c** spherical γ' precipitates
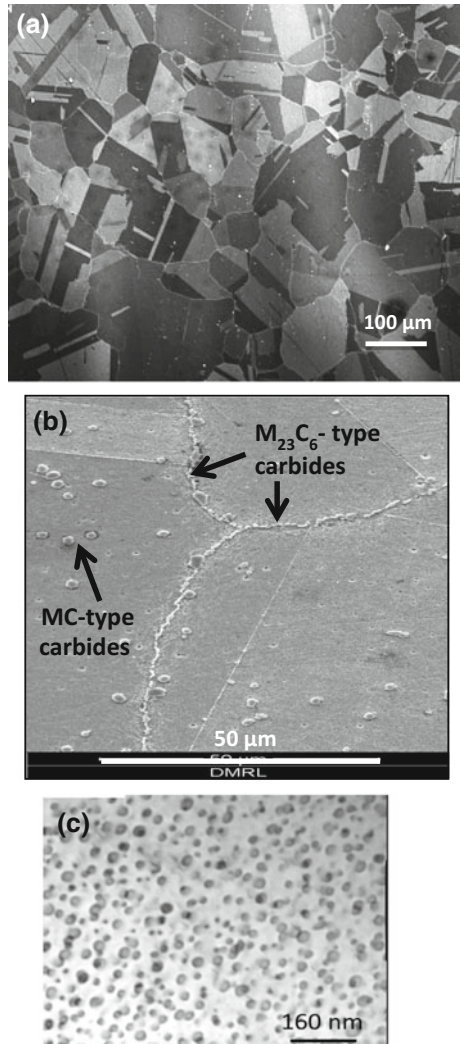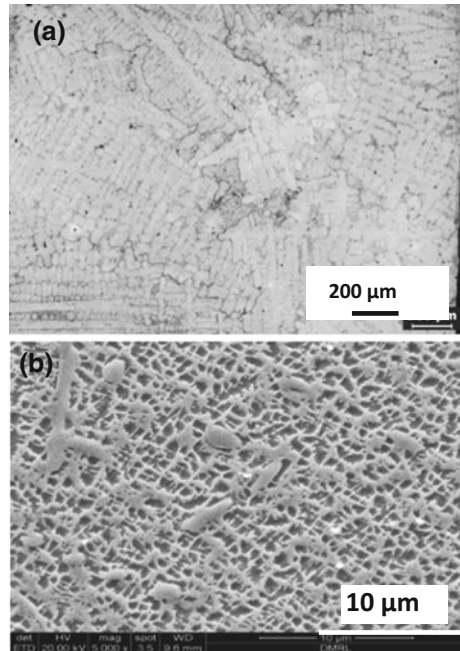
Fig. 9.4 Cast alloy microstructures: **a** dendrites within coarse equiaxed grain structure **b** coarse MC-type (TiC) carbides and near cuboidal γ′ precipitates within grains

9.3.4 Strengthening Mechanisms

Nickel-based superalloys consist of matrix γ containing a dispersion of ordered intermetallic precipitates of the type Ni_3Al (γ′). To increase the strength of initial simple Ni–Cr–Al–Ti alloys, the approach has been to strengthen the matrix by adding other elements that can be taken into substitutional solid solution and to increase the volume fraction of γ′.

The grain boundaries are reinforced by carbide precipitation and by the use of minor additions of boron and zirconium to increase grain boundary cohesion. This strengthening method obviously does not apply for SCs.

Because of its electronic structure, the fcc nickel lattice enables a larger solubility for many other elements [3–5]. Solid solution strengthening is partly caused by lattice distortion and therefore increases with increase in atomic size difference up to a maximum of about 10 %. High melting point elements provide strong lattice cohesion and reduce diffusion, particularly at high temperatures. Mo and W are particularly effective for both these reasons.

Atomic clustering or short range order can also strengthen the matrix. This is an electronic effect and is observed with Mo, W, Cr, and Al. These elements therefore produce greater hardening than Fe, Ti, Co, or V. However, strengthening due to short range order diminishes rapidly above about 0.6 T_m owing to increased diffusion.

Fig. 9.5 a Scanning electron
micrograph of a typical single
crystal microstructure,
cuboidal γ′-precipitates
surrounded by γ-matrix, **b** fcc
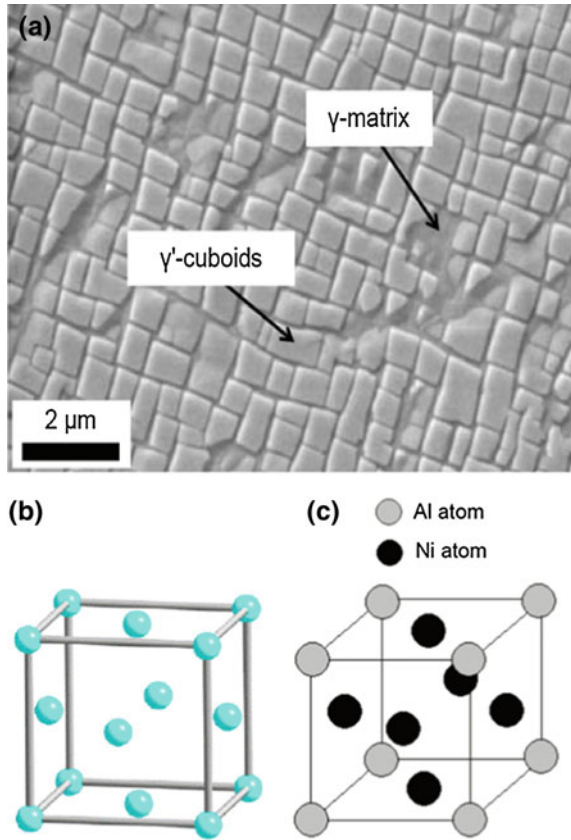gamma structure and,
c L12-ordered crystal
structure of γ′-phase

Table 9.4 Typical heat treatment cycles for various types of nickel-based superalloys

Alloy	Alloy type	Heat treatment cycle
IN718	Wrought	980 °C/1 h/AC-720 °C/8 h-FC-620 °C/8 h/AC
Udimet 720		1113 °C/2 h/AC-1079 °C/4 h/OQ-649 °C/24 h-760 °C/8 h
Mar-M-200	Cast: equiaxed grain structure	1230 °C/1 h-1260 °C/0.5 h-1080 °C/8 h-870 °C/15 h
DS CM 247	Cast: directionally solidified	1230 °C/1 h-1260 °C/3 h/Argon quench-1080 °C/4 h/Argon quench-870 °C/20 h/AC
AM1	Cast: single crystal	1300 °C/3 h/Argon quench-1100 °C/9 h/Argon quench-870 °C/20 h

AC air cooled; *FC* furnace cooled; *OQ* oil quenched

The origin of precipitation hardening is complex. The size and spacing of the
precipitates and therefore their volume fraction are important factors [3–5].
Generally, the hardening increases with increased amounts of precipitate, and it also
increases, up to a peak value, with increasing precipitate size:

- Before the age-hardening peak is reached, the operative strengthening mechanism involves cutting of γ′ particles by dislocations, and the strength increases with increasing γ′ size as shown in Fig. 9.6.
- After the age-hardening peak, the strength decreases with continuing particle growth, because dislocations no longer cut the γ′ particles but bypass them. This effect can be demonstrated for tensile or hardness behaviour in low-volume fraction γ′ alloys (A-286, Incoloy 901, Waspaloy), but may not be as readily apparent in high-volume fraction γ′ alloys such as MAR-M-247 and IN-100 [4]

For creep rupture the effects of ageing are less well defined than for short-time properties such as tensile strength. Uniform fine to moderate γ′ sizes (0.25–0.5 μm) are preferred to coarse or hyperfine γ′ for optimal creep properties. The reasons for this are related to the interactions of dislocations with matrix/precipitate interfaces and the precipitates themselves [3–5, 11, 12].

9.4 Manufacturing Processes

Superalloy ingots are subsequently used for one of three major processing routes, see Fig. 9.7. These are (1) remelting and subsequent investment casting, (2) remelting followed by wrought processing, or (3) remelting to form superalloy powder that is subsequently consolidated and subjected to wrought processing operations.

Ingots are fabricated by vacuum induction melting (VIM) in a refractory crucible to form a base alloy. Although selected alloys can be melted in air/slag environments using electric arc furnaces, VIM melting of superalloys is much more effective in the removal of low melting point trace contaminants [2–4, 11]. The

Fig. 9.6 Strength (hardness) versus particle diameter [4]. Smaller particles are cut by dislocations, but they have to bypass larger particles by bowing out between them. The result is a strength increase. Note that lower ageing temperatures increase the strength as well
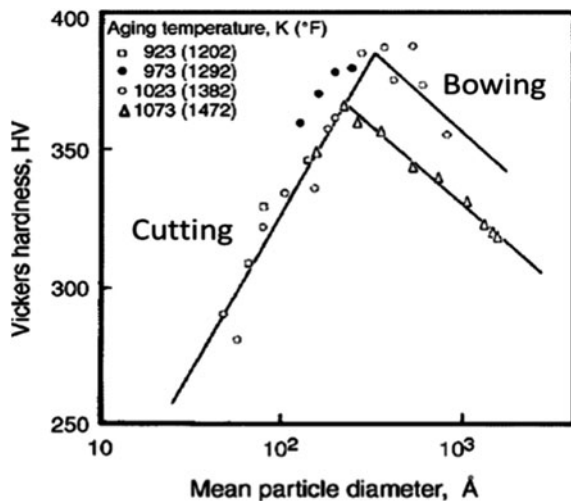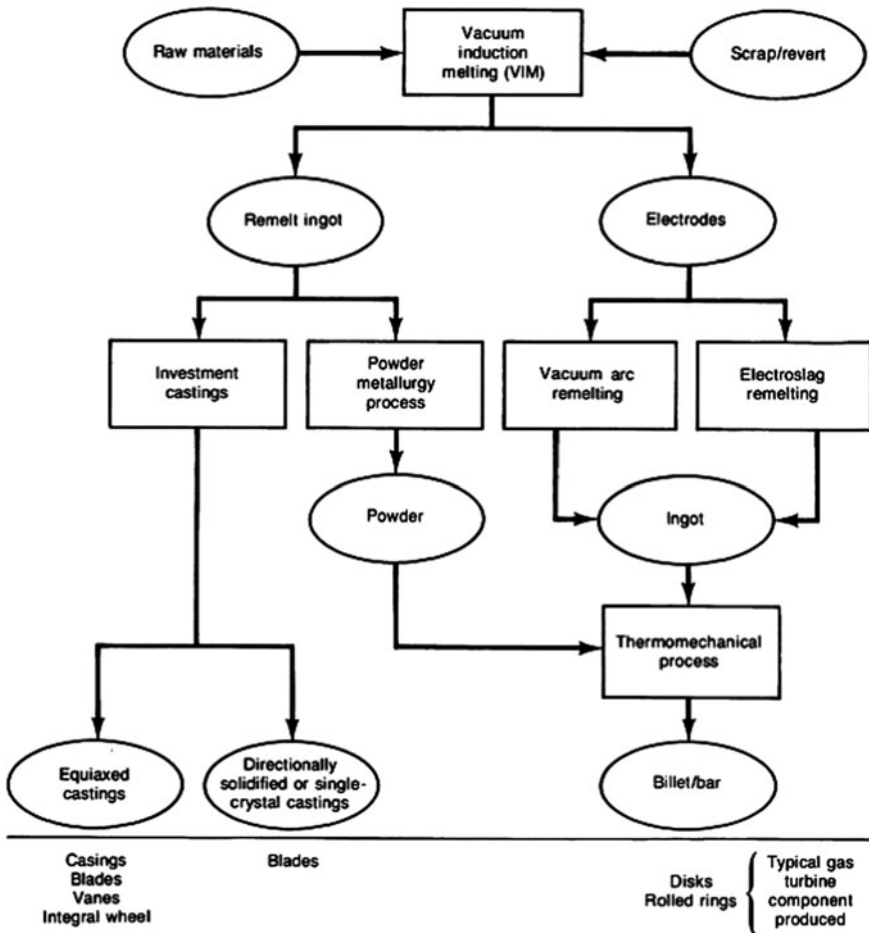
Fig. 9.7 Process flow chart illustrating manufacturing routes for superalloy products and components

alloy ingots are subsequently subjected to additional melting or consolidation processes that depend upon the final application of the material.

9.4.1 Wrought Alloys

Wrought alloys are typically fabricated by remelting of VIM ingots to form secondary ingots for subsequent deformation processing. A secondary melting process is necessary for wrought alloys because the high temperature structural properties of nickel-based superalloys are very sensitive to microstructural variations, chemical

inhomogeneities, and inclusions. As ingot sizes increase, VIM melting often results in macrosegregation or the formation of large shrinkage cavities during solidification. The formation of these solidification defects is caused by large-scale solute segregation associated with dendritic solidification under low thermal gradients. Because heat transfer during solidification of VIM ingots is limited by the low intrinsic thermal conductivity of the solidifying mass, large ingots are very prone to the formation of these defects [4, 8, 11]. Thus other secondary melting processes are utilized, including vacuum arc remelting (VAR), electro-slag remelting (ESR), and electron beam cold hearth refining (EBCHR) [4, 8, 11].

For the production of critical rotating components, such as turbine discs, VAR is used to refine the ingot and eliminate macrosegregation. Consumable electrodes (30–50 cm in diameter) cast by VIM are remelted into a water cooled copper crucible. Unlike the VIM process, in which the entire quantity of the alloy is molten and allowed to solidify, VAR involves only localized melting of the electrode tip. Melt rates of VAR are on the order of 0.5–1 kg/s. Defect features, such as macrosegregation and shrinkage, are effectively minimized since high thermal gradients are maintained during solidification of the comparatively smaller melt pool [4, 8, 11]. The remelted ingots are subsequently subjected to thermomechanical processing such as forging, hot rolling, extrusion, etc., to obtain the final products including billets, slabs, rods, plates, and sheets.

Combustor components are fabricated out of sheet nickel-based superalloys. Hastelloy X was used from the 1960–1980s. Nimonic 263 was subsequently introduced and has higher creep strength [36]. As combustion temperatures have further increased in newer gas turbines, HA-188, a cobalt-based superalloy has been recently introduced for some combustion system components for improved creep rupture strength [36].

IN 718 has been used for the manufacture of discs in aircraft engines for more than 25 years [36]. This alloy has been produced through the conventional ingot metallurgy route. IN 718 is the most frequently used superalloy for aircraft gas turbines, but because of its segregation tendency it could not be produced with ingot diameters more than 500 mm until the beginning of the twenty-first century. Remelting developments and very close control of chemical composition have enabled production of ingots as large as 750 mm in diameter. This has resulted in the ability to process IN 718 to the large disc sizes needed in modern industrial gas turbines (IGTs). A considerable amount of R&D on IN 718 has been reported at several international conferences [37–42].

Udimet 720 [43] has also evolved as an advanced wrought alloy for land-based gas turbines. Reductions in Cr content to prevent sigma phase formation and in carbon and boron levels to reduce stringers and clusters of carbides, borides, or carbonitrides, have led to the development of Udimet 720 LI. Both alloys have also been incorporated in some aircraft gas turbines [43]. The chemical compositions of Udimet 720 and 720 LI alloys may be compared from Table 9.1.

9.4.2 Cast Superalloys

The compositions of wrought alloys are restricted by the hot workability require-ments, and this has led to the development of cast alloys. The main advantage of cast alloys is that their compositions can be tailored for good high-temperature strength, since there is no forgeability requirement. Further, cast components are intrinsically stronger than forgings at high temperatures, owing to their coarse grain size. A recent review has covered the advances made in cast nickel-based super-alloys [44].

Cast IN 713 was among the early grades established as materials for airfoils in the most demanding gas turbine applications. Efforts to increase the γ' volume fraction to realize higher creep strength led to the development of alloys like IN 100 and Rene 100. Increased amount of refractory solid solution strengtheners such as W and Mo were added to some of the grades developed later, and this led to the availability of grades like MAR-M200, MAR-M246, IN 792, and M22. Subsequent addition of 2 wt% Hf improved ductility, and a new series of alloys became available, such as MAR-M200 + Hf, MAR-M246 + Hf, and Rene 125 + Hf.
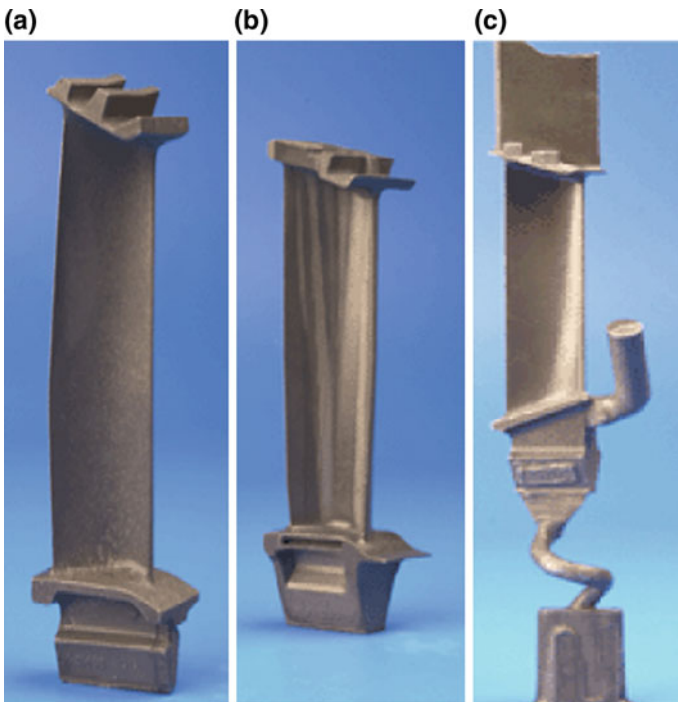

Fig. 9.8 Turbine blades: **a** equiaxed polycrystalline, **b** DS polycrystalline, and **c** single crystal, showing the as-cast component

General Electric pursued its own alloy development with Rene 41, Rene 77, Rene 80, and Rene 80 + Hf having relatively high Cr content for improved corrosion resistance at the cost of some high-temperature strength. Similar alloys with high Cr content are IN738C, IN738LC, Udimet 700, and Udimet 710. The chemical compositions of all these cast alloys are included in Table 9.2.

Investment casting [2–4, 11] is the primary casting process for fabrication of superalloy components with complex shapes, including blades and vanes. Ceramic moulds containing alumina, silica, and/or zirconia are utilized in this process. The moulds are fabricated by progressive buildup of ceramic layers around a wax pattern of the cast component. Ceramic cores can be embedded in the wax to obtain complex internal cooling structures.

A thermal cycle removes the wax, and the mould is filled with remelted superalloy in a preheated vacuum chamber to obtain a shaped casting. Castings thus obtained may be equiaxed, directionally solidified (DS) columnar grained, or single crystal (SC) (Fig. 9.8). Equiaxed castings solidify fairly uniformly throughout their volume, whereas columnar and SC castings are withdrawn from a hot zone in the furnace to a cold zone at a controlled rate. A schematic is shown in Fig. 9.9.

Following initial solidification, castings are subjected to a series of heat treatment cycles that serve to reduce segregation, establish one or more size populations of γ′ precipitates, modify the structure of grain boundary phases (particularly carbides), and/or assist in the application of coatings.

DS-induced grain defects: DS processing can result in several types of chemistry sensitive grain defects [46]. The two most common defects are freckle chains and misoriented grains (Fig. 9.10).

Freckle-type defects [45–52] occur because of convective instabilities in the mushy zone. The instabilities develop as a result of density inversions created by progressive segregation of individual alloying elements during solidification. The fluid flow within "channels" that develop because of these instabilities [53, 54] results in fragmentation of dendrite arms, producing a small chain of equiaxed grains aligned approximately parallel to the solidification direction. The freckles are enriched in elements that segregate to the interdendritic region during solidification and thus differ in composition from the base alloy [46]. Freckle formation is promoted by low cooling rates, (low thermal gradients) and corresponding large dendrite arm spacings [47].

Misoriented grains differ from freckles in that they have the same nominal composition as the base alloy, but are typically larger and elongated along the solidification direction.

The occurrence of these defects can be avoided by reducing the *density gradient* in the mushy zone, which is accomplished by increasing the thermal gradient in the process [46–49]. There has recently been greater effort aimed at increasing the thermal gradients. A new approach involves the use of liquid-metal coolants (LMCs) during solidification [53]. A modified Bridgman system using liquid tin as a cooling medium has been developed. Substantial increases in cooling rate and elimination of freckle defects have recently been demonstrated by this method [54].

Fig. 9.9 Schematics of typical DS process (*top*) and the beginning of the single crystal DS process (*bottom*), whereby a helical mould section prevents all but one grain from growing into the main casting
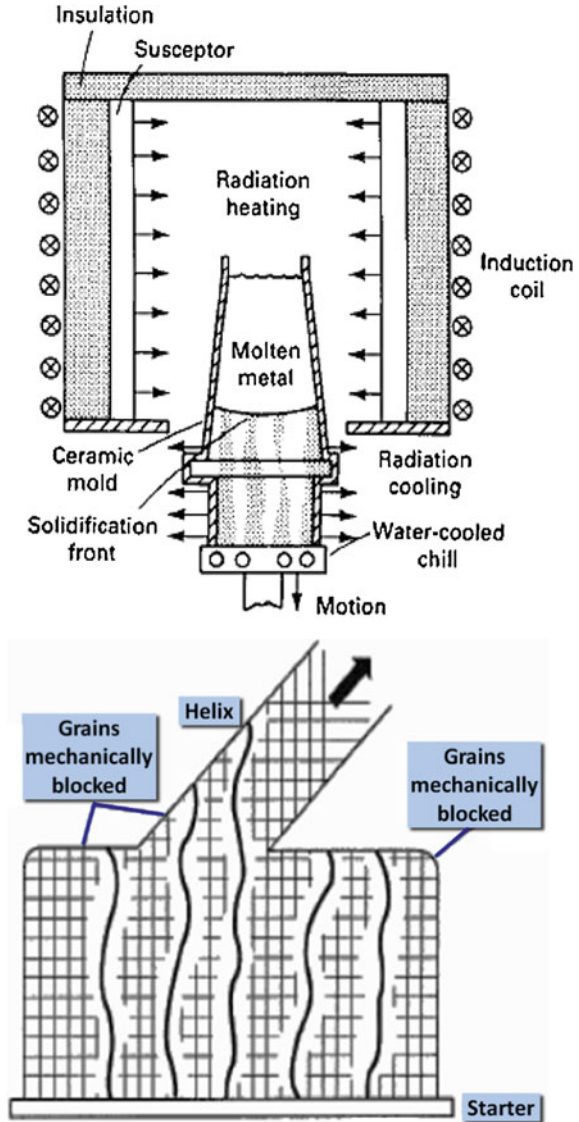
9.5 Properties of Superalloys

Superalloys constitute a large fraction of the structural materials in turbine engines because of their unique combination of physical and mechanical properties. Table 9.5 lists some typical physical properties of superalloys. In aircraft engines, it is typical to consider density normalized properties, especially in rotating
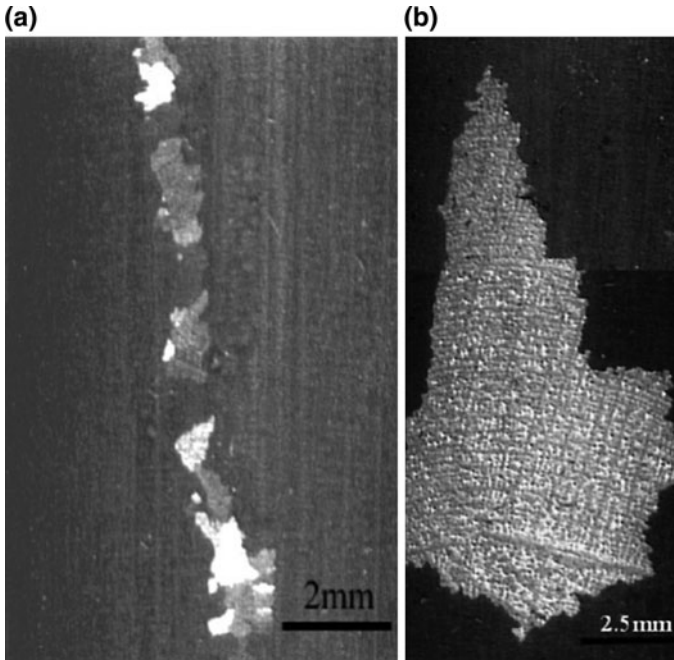
Fig. 9.10 Macroscopic chemistry-sensitive grain defects present on the surfaces of single crystal nickel-based superalloy castings: **a** freckles and **b** a misoriented grain

components. Thus alloy densities, which are typically in the range of 7.7–9.0 g/cm^3, are of particular interest.

Optimization of mechanical properties is of paramount importance and depends on a high level of control and understanding of the processes mentioned in Sect. 9.4. Mechanical properties of primary interest include tensile properties, creep, fatigue, and cyclic crack growth. Depending on the details of component design, any one of these four properties may be life-limiting.

9.5.1 Tensile Properties

Nickel-based superalloys have relatively high yield and ultimate tensile strengths, often in the respective ranges of 900–1300 MPa and 1200–1600 MPa at room temperature. Figure 9.11 shows the temperature dependence of the yield strength of an SC alloy and a PM-processed disc alloy [11, 55, 56]. The blade alloy tensile properties do not substantially decay until temperatures above 850 °C. However, disc alloys are typically developed to have higher strengths at temperatures below 800 °C, with some design margin in strength to protect against disc burst in the event of an engine overspeed.

Table 9.5 Physical properties of nickel-based superalloys

| Properties	Typical ranges and values
Density	7.7–9.1 g/cm^3
Melting point	1320–1450 °C
Elastic modulus	RT: 210 MPa
	800 °C: 160 MPa
Thermal expansion coefficient	8–18 × 10^{-6}/°C
Thermal conductivity	RT: 11 W/m.K
	800 °C: 22 W/m.K

Figure 9.11 also shows that the yield strengths increase slightly at intermediate temperatures. This unusual behaviour is due to the complicated dislocation movements required to shear the γ′ precipitates in this temperature range [5, 57–59]. Note also from Fig. 9.12 that a two-phase superalloy is much stronger than either the matrix or precipitate materials in their bulk form.

9.5.2 Creep Resistance

Gas turbine components experience stresses at high temperature for extended periods. Hence a high resistance to creep deformation is essential. This is very important for cast blade alloys, because they are exposed to temperatures up to 1100 °C, whereas disc alloys are typically limited to less than 700 °C.

For a fixed stress and temperature precipitate-strengthened superalloys have much higher creep resistance than their single-phase counterparts. It has been reported that the strength peaks when the precipitate volume fractions are in the range of 0.6–0.7, and many advanced alloys contain precipitates in this range [60].

Fig. 9.11 Temperature dependence of yield strength for a single crystal turbine blade alloy and a PM polycrystalline disc alloy
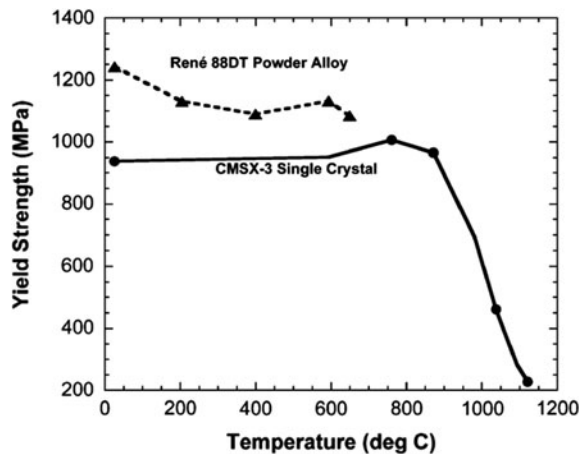
Alloy chemistry is also important to creep properties. Because the rate-controlling processes in creep are diffusion-controlled, elements that have low interdiffusion coefficients with nickel are generally beneficial. Elements most effective at slowing diffusion include Ir, Re, Ru, Pt, W, Rh, and Mo [61, 62]. Advanced creep-resistant alloys benefit from substantial additions of Re, W, and Mo (Tables 9.2, 9.6, 9.7, 9.8 and 9.9).

A combination of increasing additions of refractory elements and advances in processing has resulted in substantial increases in the maximum temperature capability of superalloys since the 1950s (Fig. 9.13). For a creep rupture life of 1000 h at a stress of 137 MPa, the most recently developed single crystal super-alloys [63, 64] have a temperature capability of approximately 1100 °C, whereas conventionally cast equiaxed alloys had a temperature capability of 900–950 °C. In fact, the temperature capabilities of advanced superalloys have now reached 85–90 % of the melting point, which is truly remarkable.

9.5.3   Fatigue

Turbine components also experience significant fluctuations in stress and temperature during their repeated start—flight operation—shutdown cycles. These cycles can result in localized small plastic strains. Thus low cycle fatigue is of interest to engine design and operation; and engine vibrations and gas/airflow fluctuations between turbine stages can also result in high cycle fatigue, with rapid cycle accumulation in airfoils at frequencies in the kHz range.

Figure 9.14 shows the conventional smooth-specimen S-N fatigue properties of the PM disc alloy Rene 88 DT at room temperature and 593 °C [65]. In the low cycle fatigue regime (typically up to about 20,000 cycles) such disc alloys exhibit

Fig. 9.12 Temperature dependence of flow stress for an as-cast and heat treated nickel-based superalloy, and the individual phases [60]
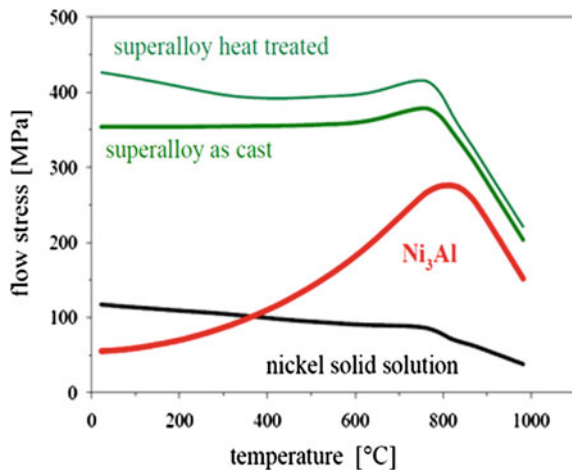
Table 9.6 Chemical compositions (wt%) of first generation single crystal nickel-based superalloys

Alloy	Cr	Co	Mo	W	Al	Ti	Ta	Nb	V	Hf	Density (g/cm^3)
CMSX-2	8	4.6	0.6	8	5.6	1	6	–	–	–	8.6
PWA 1480	10	5	–	4	5	1.5	12	–	–	–	8.7
SRR 99	10	5	–	10	5.5	2.2	3	–	–	–	8.56
Rene N4	9	8	2	6	3.7	4.2	4	0.5	–	–	8.56
AM1	7.8	6.5	2	5.7	5.2	1.1	7.9	–	–	–	8.6

Table 9.7 Chemical compositions (wt%) of second generation single crystal nickel-based superalloys

Alloy	Cr	Co	Mo	Re	W	Al	Ti	Ta	Nb	Hf	Density (g/cm^3)
CMSX-4	6.5	9	0.6	3	6	5.6	1	6.5	–	0.1	8.7
PWA 1484	5	10	2	3	6	5.6	–	8.7	–	0.1	8.95
Rene N5	7	8	2	3	5	6.2	–	7	–	0.2	8.7
MC2	8	5	2	–	8	5	1.5	6	–	–	8.63

Table 9.8 Chemical compositions (wt%) of third generation single crystal nickel-based superalloys

| Alloy	Cr	Co	Mo	Re	W	Al	Ti	Ta	Nb	Hf	Others	Density (g/cm^3)
CMSX-10	2	3	0.4	6	5	5.7	0.2	8	0.1	0.03	–	9.05
Rene 6	4.2	12.5	1.4	5.4	6	5.75	–	7.2	–	0.15	0.05 C; 0.004 B 0.01 Y	8.97
TMS-75	3	12	2	5	6	6	–	6	–	0.1	–	–

outstanding fatigue properties, with fatigue strengths that are a high fraction of the monotonic yield strength.

The variability (scatter) in fatigue lives increases at lower stresses and longer lives. This is also shown in Fig. 9.14, where fatigue lives at 593 °C vary between approximately 10^6 cycles and 10^9 cycles. The scatter is probably caused by differences in the fatigue crack initiation lives. In turn, these differences can be due to intrinsic variations in microstructure [65–69] and/or the infrequent presence of PM-induced discontinuities (defects). In cast alloys fatigue cracks may also initiate at porosity, carbides, or eutectic.

Table 9.9 Chemical compositions (wt%) of fourth, fifth, and sixth generation single crystal nickel-based superalloys

Alloy	Cr	Co	Mo	Re	W	Al	Ru	Ta	Hf	Others	Density (g/cm^3)	Alloy Generations
EPM-102	2	16.5	2	5.95	6.0	5.6	3.0	8.25	0.15	0.03 C 0.004 B 0.001 Y	9.2	Fourth
TMS-138	3.2	5.8	2.9	5	5.9	5.8	2.0	5.6	0.1	–	8.95	
Tms-138A	3.2	5.8	2.9	5.8	5.6	5.7	3.6	5.6	0.1	–	9.01	
TMS-162	3.0	5.8	3.9	4.9	5.8	5.8	6.0	5.6	0.1	–	9.04	Fifth
TMS-173	3.0	5.6	2.8	6.9	5.6	5.6	5.0	5.6	0.1	–	9.11	
TMS-196	4.6	5.6	2.4	6.4	5.0	5.6	5.0	5.6	0.1	–	9.01	
TMS-238	4.6	6.5	1.1	6.4	4.0	5.9	5.0	7.6	0.1	–		Sixth

Fig. 9.13 Illustration of the enhancement of creep performance of nickel-based superalloys from the 1950s to the present, owing to casting technology developments
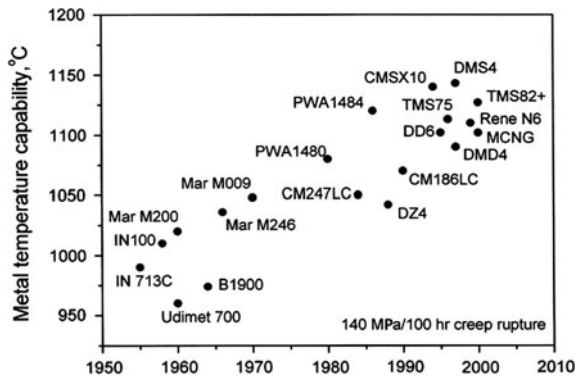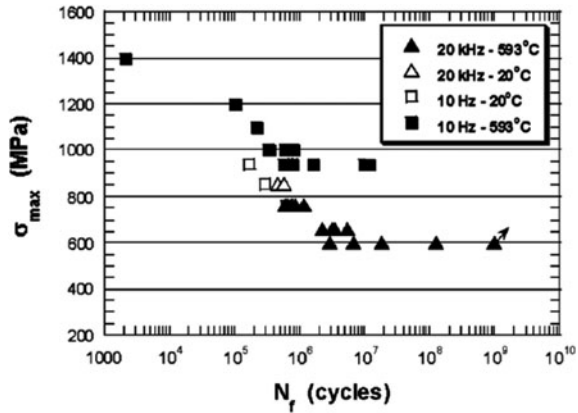

9.5.4 Fatigue Crack Growth

Fatigue crack propagation is also an important aspect of superalloy behaviour, particularly for turbine disc materials. So-called 'Paris Law' crack growth behaviour is displayed over a wide range of stress intensity factor ranges (ΔK) for most superalloys [66, 67, 69]. The fatigue crack growth threshold ΔK values (ΔK_{th}) [70] are relatively high and often above 8 MPa.m$^{1/2}$.

The crack growth rates are sensitive to microstructural features, including grain sizes, precipitate sizes, and volume fractions of precipitates [70]. At temperatures above about 500 °C environmental and cycle frequency effects become significant factors, with higher crack growth rates in air than *in vacuo* or in inert environments [4].

In single crystal superalloys, cracks may grow crystallographically along {111} planes, particularly in the early stages of growth (stage I) [7, 70]. Depending on

Fig. 9.14 Fatigue (S-N) behaviour of PM Rene 88 DT at 20 and 593 °C at a load ratio of 0.05 and frequencies of 10 Hz and 20 kHz. The arrow shows a specimen runout beyond 10^9 cycles

testing conditions, as cracks grow longer (stage II) there is a greater tendency toward mode 1 behaviour [68, 71].

Because fatigue and fatigue crack growth are often limiting properties, comprehensive models for life prediction that account for complex loading, crack initiation and crack growth, as well as microstructural and environmental effects, continue to be developed. The integration of physics-based models with advanced sensors that can diagnose the current "damage state" is a promising approach for life prediction [72].

9.6 Evolution of Advanced Nickel-Based Superalloys

In the case of cast superalloys, the introduction of directionally solidified (DS) columnar grained blades led to considerable increases in creep strength owing to the elimination of transverse grain boundaries. SC castings were developed during the 1970s and were a spin-off from the technological advances made in the DS casting processes. SC castings are produced in a similar fashion to DS by selecting a single grain via a grain selector, see Figs. 9.8 and 9.9. During solidification, this single grain grows to encompass the entire part.

Even more spectacular improvements in creep strength became possible for SC castings, since besides the total elimination of grain boundaries, the chemistries could be altered (rebalanced) to increase the solidus temperature beyond the γ' solvus. This avoided the formation of eutectic nodules and made it possible to use high temperature homogenization, with complete solutionizing of the γ' and subsequent formation of a uniform distribution of fine precipitates.

In slightly more detail, the exceptional properties of DS and SC alloys are due to [4, 11, 15]:

1. The alignment or elimination of any weak grain boundaries oriented transverse to the loading direction.
2. The low modulus associated with aligning the $\langle 100 \rangle$ crystallographic directions parallel to the blade or vane spans enhances the thermomechanical fatigue resistance in areas of constrained thermal expansion, particularly for turbine vanes.

In general, the lack of transverse grain boundaries coupled with the lower modulus can result in 3–5 times improvement in creep rupture life.

As should be evident from subsection 9.4.2, the manufacture of advanced SC blades is a high-precision casting process. Many of the early DS blades produced from the late 1960s were hollow, with air cooling channels about half a millimetre in diameter [3–5]. Today's SC blades often contain even more intricate cooling circuits, and the wall thickness can be as small as a few tenths of a millimetre. These developments have resulted in progressively higher operating temperatures, as was already shown in Fig. 9.13.

The SC superalloys are often classified into first, second, third, fourth, and fifth generation alloys. The evolution of these alloys is summarized in Sects. 9.6.1–9.6.6. Also, Tables 9.5, 9.6, 9.7, and 9.8 give the chemical compositions and densities of a few SC alloys from each generation.

9.6.1 First Generation Superalloys

These alloys were derived from wrought superalloys to take advantage of vacuum melting and casting introduced in the early 1950s. All these cast superalloys can be grouped into conventionally cast (CC), DS and SC superalloys.

Important aspects of alloy development toward improving the strength of the alloys include introduction of higher γ' contents, elimination of formation of deleterious phases such as σ and Laves phases using phase computation (PHACOMP [73] and Calphad [32–35]), improved castability through additions of Ta, increased additions of refractory solid solution strengtheners (such as W and Mo) to impart higher temperature capability, and addition of Hf (~ 2 wt%) to improve stress rupture ductility and minimize porosity via increased amounts of low melting point eutectic.

Subsequently, elimination of transverse grain boundaries by direct solidification (DS) of blades and vanes led to a further improvement in temperature capability. Although transverse grain boundary elimination was the original motivation for DS, it was the favoured $\langle 100 \rangle$ growth directions and improved heat treatment characteristics from which most benefits occurred. Alignment of a $\langle 100 \rangle$ direction along the blade span not only provided intrinsically high creep resistance, but also greatly improved the thermal fatigue life, since this is a low Young's modulus direction [4, 7, 9].

DS turbine blades and vanes began appearing in military and commercial aeroengines in the 1960s. A logical extension of eliminating transverse grain boundaries in DS technology was to remove grain boundaries altogether to produce SC blades and vanes.

9.6.2 Second Generation Superalloys

The development of second generation SC alloys [10–16], which are essentially rhenium (Re)-modified ($\sim$3 wt%, see Table 9.7), was marked by increased additions of refractory alloying elements, while maintaining a γ' volume fraction above 60 %.

Re is known to partition mainly to the γ-matrix, to retard γ' coarsening, and to increase the γ'/γ misfit. It is argued that some of the enhanced resistance to creep comes from the promotion of γ' 'rafting' by Re [14–16]. It is also claimed that Re reduces the overall diffusion rate in nickel-based superalloys [10–16].

In summary, the second generation SC alloys provide about a 30 °C metal operating temperature improvement, together with adequate resistance to oxidation, thermal fatigue and deleterious phase formation relative to the first generation SC alloys.

9.6.3 Third Generation Superalloys

The development of third generation superalloys [17–19] was marked by yet higher additions of Re ($\sim$6wt%, see Table 9.8) due to its dual role of improving creep strength as well as environmental resistance in spite of a low Cr level. Development of these alloys has led to yet another 30 °C improvement in metal operating temperature capability, this time relative to the second generation superalloys. Some examples follow:

1. Cannon Muskegon Corporation, USA, optimized their third generation SC alloy CMSX10 employing total refractory elements of about 20 wt%, with 6 wt% Re after tailoring the Cr, Co, and W levels to 2, 3, and 5 wt%, respectively [17, 18].
2. GE designed an SC superalloy, Rene 6, with optimized composition to have a good balance between stress rupture strength and microstructural stability [19]. This overcame the problem of TCP formation in CMSX10 during long-term exposure at higher temperature.
3. An SC superalloy DMS4 [74] was developed at DMRL, India, by pushing the total refractory element content to 22 wt%, with about 6.5 wt% Re and removing Mo and Ti completely. This alloy exhibits superior strength together with good castability, alloy phase stability, and environmental resistance.

4. Further, a columnar grained superalloy DMD4 [74] was derived from the DMS4 alloy for cost competitive production of complex turbine airfoils, which are difficult to cast in SC form. The alloy composition has been tailored by replacing some of the Ta with Hf and incorporating C and B for grain boundary strengthening. The alloy also had good phase stability, environmental resistance, and creep rupture properties close to those of the *second generation SC* superalloy CMSX-4.

9.6.4 Fourth Generation Superalloys

The fourth generation superalloys, Table 9.9, were developed by the additions of platinum group metals (PGMs), especially ruthenium (Ru), to third generation superalloys to further improve the phase stability in the presence of higher refractory element contents, thereby improving the strength [20–23]. Further, the higher negative γ/γ′ misfit resulted in γ′ rafting perpendicular to the applied stress, thereby acting as a barrier to deformation under high temperature and low stress conditions.

9.6.5 Fifth Generation Superalloys

The fifth generation superalloys [24, 25] was developed with yet higher Ru contents (≥6 wt%). TMS-162 and TMS-172 are the first two fifth generation SC superalloys (Table 9.9) developed by the National Institute of Materials Science (NIMS) [25] and have excellent creep resistance.

Higher Ru contents (≥5 wt%) allow higher Mo and Re additions in TMS-162 and TMS-173, respectively. Higher lattice misfit and further solid solution strengthening by Mo and Re as well as Ru, and improved phase stability by Ru can all contribute to superior creep resistance over the previous generations. However, the lower Cr content of these two alloys has resulted in poorer oxidation resistance at elevated temperatures, owing to vaporization of Ru and Re oxides [25].

On the other hand, another fifth generation superalloy, TMS-196, with a moderate amount of Cr, exhibits acceptable oxidation resistance similar to that of Rene N5. Also, TMS-196 possesses better microstructural stability and shows significant improvements in creep resistance and thermal fatigue properties over the current commercial superalloys such as CMSX-4, CMSX-10, PWA1484, and Rene N5 [25].

9.6.6 Sixth Generation Superalloys

As can be seen from Table 9.9, the fifth generation SC superalloy TMS-196 has higher contents of Re and Ru as compared to the fourth generation superalloy TMS-138A. These changes were made in order to obtain better mechanical properties [26]. TMS-196 also has better oxidation properties due to its higher Cr content.

Continuing the developments, NIMS have recently developed yet another advanced alloy, TMS-238, with mechanical properties similar to those of TMS-196 but with improved oxidation and hot corrosion resistance.

For TMS-238 the Mo and W contents were reduced and the Co and Ta contents were increased, as can be seen in Table 9.9. The tensile properties of this sixth generation superalloy are given in Table 9.10, and it is claimed that these properties are superior to those of all other generations of superalloys.

The creep rupture properties of TMS-238 at 800, 900, and 1000 °C are comparable to those of TMS-138A and TMS-196, but at 1100 °C TMS-238 is superior, see Fig. 9.15. TMS-238 alloy also has superior oxidation properties, and thus an unmatched combination of mechanical and environmental properties [26].

Table 9.10 Tensile properties of various generations of single crystal nickel-based superalloys

Alloy and generation	400 °C		750 °C	
	0.2 % yield strength (MPa)	UTS (MPa)	0.2 % yield strength (MPa)	UTS (MPa)
CMSX-4: II	860	950	950	1150
TMS-138A: IV	830	906	868	1241
TMS-196: V	879	1214	845	1308
TMS-238: VI	925	1373	1041	1348

Fig. 9.15 Comparison among different generations of nickel-based superalloys in terms of 1100 °C/137 MPa creep and 1100 °C oxidation resistance [26]
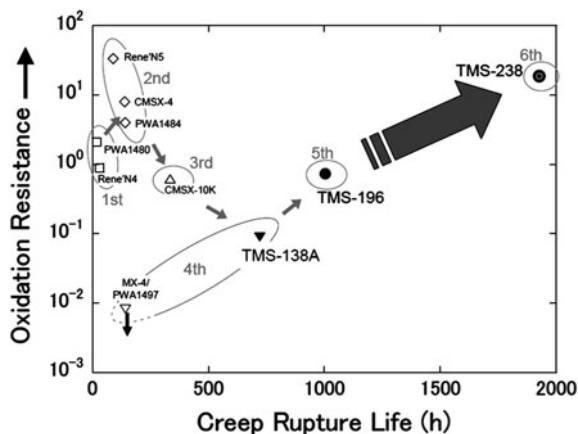
9.7 Concluding Remarks

The ordered gamma prime (γ'), which is the main source of strengthening, endows nickel-based superalloys with exceptional performance and renders them superior to most of the other high temperature structural alloys. This is because γ' is stable up to temperatures of 1000 °C and can directionally coarsen under service conditions for enhanced creep resistance.

The performances of the superalloys have progressively improved by controlling chemistry and microstructure, and by innovative processing technologies. Surface modification by application of coating technology concurrent with the introduction of directionally solidified (DS) structures and then single crystals (SCs), has extended the useful temperature range of superalloys. In spite of considerable recent efforts toward developing other materials such as intermetallics, ceramics, and their composites for engine applications, nickel-based superalloys continue to be the most reliable materials for hot sections of turbines.

Six generations of SC nickel-based superalloys with improved creep properties and phase stability have already been developed. Therefore it appears that the evolution of advanced nickel-based superalloys is a never-ending process, and their replacement in turbine engine applications seems to be impossible at least for the next few decades.

References

1. Betteridge W (1974) The Nimonic alloys, and other Nickel-base high temperature alloys. In: Betteridge W, Heslop J (eds) Edward Arnold, London, UK
2. Sims CT, Stoloff NS, Hagel WC (1987) Superalloys II. Wiley, Hoboken, NJ, USA
3. Meetham GW, Van de Voorde MH (2000) Materials for high temperature engineering applications. Springer-Verlag, Berlin, Germany
4. Donachie MJ, Donachie SJ (2002) Superalloys: a technical guide, 2nd edn. ASM International. Materials Park, OH, USA
5. Reed RC (2006) The superalloys: fundamentals and applications. Cambridge University Press, Cambridge, UK
6. Muktinutalapati NR (2011) Materials for gas turbines—an overview, advances in gas turbine technology. Benini E (ed). Intech Open Source Publisher: book.department@intechopen.com, pp 293–314
7. MacKay A, Gabb TP, Smialek JL, Nathal MV (2009) Alloy design challenge: development of low density superalloys for turbine blade applications. Rebecca Glenn Research Center, Cleveland, Ohio 44135, NASA/TM—2009-215819
8. Caron P, Khan T, Evolution of Ni-based superalloys for single crystal gas turbine blade applications. Aerosp Sci Technol 3(8):513–523
9. Khan T (1986) High temperature alloys for gas turbines and other applications. In: Betz W et al (eds) D. Reidel Publishing Company, Dordrecht, Holland, p 21

10. Cetel AD, Duhl DN (1992) Second generation columnar grain Nickel-base superalloy. In: Antolo SD, Stusrud RW, MacKay RA, Anton L, Khan T, Kissinger RD, Klarstrom L (eds) Superalloys 1992, TMS, Warrendale, PA, USA, pp 287–296
11. Pollock TM, Tin S (2006) Propulsion and power, vol 22, 2, p 361
12. Diego Colombo (2006–2007) Nickel-based superalloys and their application in the aircraft industry. Anno accademico, Universita Deglistudi Di Trento, Italy
13. Caron P, Lavigne O (2011) Recent studies at onera on superalloys for single crystal turbine blades. J Aerosp Lab 3, pp 1–14
14. Second Generation single crystal superalloy(Developed under NIMS1/Toshiba2 collaboration), High Temperature Materials Group, Materials Engineering Laboratory (MEL), National Institute for Materials Science(NIMS), Japan, August, 2004
15. Li JR, Zhong ZG, Tang DZ, Liu SZ, Wei P, Wei PY, Wu ZT, Huang D, Han M (2000) A Low-cost second geneution single crystal superalloy DD6. In: Pollock TM, Kissinger RD, Bowman RR, Green KA, McLean S, Olson, Schina JJ (eds) Superalloys 2000, TMS, Warrendale, PA, USA, pp 777–783
16. Cetel AD, Duhl DN (1988) Second generation nickel base single crystal superalloy. In: Reichman S, lhhl DN, Maurer G, Antolovich, S, Lund C (eds) Superalloys 1988, TMS, Warrendale, PA, USA, pp 235–244
17. Ericson Gary L, JOM BS (2006) A new third generation, single crystal, casting superalloy 47 (5):36–39
18. Walston S, O'Hara, KS, Ross EW, Pollock TM, Murphy WH (1996) RENE N6: third generation single crystal superalloy. In: Kissinger RD, Deye DJ, Anton DL, C&l AD, Nathal MV, Pollo TM, Woodford DA (eds) Superalloys 1996, TMS, Warrendale, PA, USA, pp 27–34
19. Caron P, Khan T (1996) Evolution of Ni-based superalloys for single crystal gas turbine blade applications. Office National d'Etudeset de Recherches Aérospatiales (ONERA), BP72 - 92322, Châtillon Cedex, France
20. Zietara M, Ceteland A, Czyrska-Filemonowicz A (2011), Microstructure stability of 4th generation single crystal superalloy, pwa 1497, during high temperature creep deformation. Materials Transactions, vol 52, no 3, pp 336–339
21. Walston S, Cetel A, MacKay R, O'Hara K, Duhl D, Dreshfield R (2004) Joint development of a fourth generation single crystal superalloy. In : 10th international symposium on superalloys cosponsored by the seven springs international symposium committee. The Minerals, Metals, and Materials Society (TMS), the TMS High Temperature Alloys Committee, and ASM International Champion, PA, USA, pp 19–23
22. Kawagishi Kyoko, Harada Hiroshi, Sato Akihiro, Kobayashi Toshiharu (2006) JOM 58 (1):43–46
23. Sato A, Yeh AC, Kobayashi T, Yokokawa T, Harada H, Murakumo T, Zhang JX (2007) Energy materials 2(1):19–25
24. Sato A, Harada H, Yeh A-C, Kawagishi K, Kobayashi T, Koizumi Y, Tadaharu Y, Zhang J-X (2008) A 5th generation SC superalloy with balanced high temperature properties and processability. In: Reed RC, Green KA, Caron P, Gabb, Fahrman MG, Huron ES, Wodard SA (eds) Superalloys 2008, TMS, Warrendale, PA, USA, pp 131–138
25. Nickel base single crystal superalloys, TMS-196, July, 2008, High temperature materials center, National Institute for Materials Science, Japan
26. Kawagishi K, Yeh A-C, Yokokawa T, Kobayashi T, Koizumi Y, Harada H (2012) Development of an oxidation resistant high strength sixth generation SC superalloy. In: 12th international symposium on superalloys. In: Huron ES, Reed RC, Hardy MC, Mills MJ, Montero RE, Portella PD, Telesman J (eds) TMS, Warrendale, PA, USA, pp 189–195
27. Ross EW (1967) Rene 100-a sigma-free turbine blade alloy. J Met 19(12):12–14
28. Nystrom JD, Nystrom TM, Murphy WH, Garg A (1997) Discontinuous cellular precipitation in a high-refractory nickel-base superalloy. Metall Mater Trans 28A:2443–2452
29. Wlodek ST (1964) The structure of IN100. Trans ASM 57:110–119

30. Rae CMF, Reed RC (2001) The precipitation of topologically close-packed phases in rhenium-containing superalloys. Acta Mater 49(10):4113–4125
31. Darolia R, Lahrman DF, Field RD (1988) Formation of topologically closed packed phases in nickel base single crystal superalloys. TMS, Warrendale, PA, USA, pp 255–264
32. Agren J (1996) Calculation of phase diagrams: Calphad. Curr Opin Solid State Mater Sci 1:355–360
33. Kattner UR (1997) Thermodynamic modeling of multicomponent phase equilibria. J Met 49 (12):14–19
34. Saunders N, Fahrmann M, Small CJ (2000) The application of CALPHAD calculations to Ni-Based superalloys. Superalloys 2000. TMS, Warrendale, PA, USA, pp 803–811
35. Wu K, Chang YA, Wang Y (2004) Simulating interdiffusion microstructuresin Ni–Al–Cr diffusion couples: a phase field approach coupled with calphad database. ScriptaMaterialia 50:1145–1150
36. Schilke PW (2004) Advanced gas turbine materials and coatings. Available at www.Gepower.com/prod-serv/products/tech-docs/en/downloads/ger3569.pdf
37. Loria ED (1989) Proceedings of conference on superalloy 718—metallurgy and applications, TMS, Warrendale, PA, USA
38. Loria ED (1991) Proceedings of conference on superalloy 718, 625 and various derivatives. TMS, Warrendale, PA, USA
39. Loria ED (1994) Superalloys 718, 625, and various derivatives. The Minerals, Metals & Materials Society, Warrendale, PA, USA
40. Loria ED (1997) Superalloys 718, 625, 706 and various derivatives. The Minerals, Metals & Materials Society. Warrendale, PA, USA
41. Loria ED (2001) Proceedings of the fifth international conference on superalloys 718, 625, 706 and various derivatives. TMS, Warrendale, PA, USA
42. Loria ED (2005) Proceedings of sixth international symposium on superalloys 718, 625, 706 and derivatives. TMS, Warrendale, PA, USA
43. Furrer D, Fecht H (1999) JOM, vol 51, 1, pp 14–17
44. Das N, Trans. IIM, vol 63, 210, pp 265–274
45. Tien JK, Caulfield T (1988) Superalloys, supercomposites and superceramics. Academic Press, New York, USA
46. Tin S, Pollock TM, Murphy W (2001) Stabilization of thermosolutal convective instabilities in Ni-based single crystal superalloys: carbon additions and freckle formation. Metall Mater Trans 32A(7):1743–1753
47. Tin S, Pollock TM (2004) Predicting freckle formation in single crystal Ni-base superalloys. J Mater Sci 39(24):7199–7205
48. Beckermann C, Gu JP, Boettinger WJ (2000) Development of a freckle predictor via rayleigh number method for single-crystal superalloy castings. Metall Mater Trans 31A(10):2545–2557
49. Wang W, Lee PD, McLean M (2003) A model of solidification microstructures in Nickel-Based superalloys: Predicting primary dendrite spacing selection. Acta Mater 51 (10):2971–2987
50. Pollock TM, Murphy WH (1996) The breakdown of solidification in high refractory nickel-base superalloys. Metall Mater Trans 27A(4):1081–1094
51. Giamei AF, Kear BH (1970) Nature of freckles in nickel-base superalloys. Metall Trans A 1:2185–2192
52. Copley SM, Giamei AF, Johnson SM, Hornbecker MF (1970) Origin of freckles in unidirectionally solidified castings. Metall Trans A 1(8):2193–2204
53. Giamei AF, Tschinkel JG (1976) Liquid metal cooling—a new solidification technique. Metall Trans A 7A:1427–1434
54. Elliott AJ, Tin S, King WT, Huang SC, Gigliotti MFX, Pollock TM (2004) Directional solidification of large superalloy castings with radiation and liquid-metal cooling: a comparative assessment. Metall Mater Trans A 35A(10):3221–3231
55. Huron ES (1992) Serrated yielding in a nickel-base superalloy. TMS, Warrendale, PA, USA, pp 675–684

56. Pollock TM, Field RD (2002) Dislocations and high temperature plastic deformation of superalloy single crystals. In: Nabarro FRN, Duesbery MS (eds) Dislocations in solids, vol 11. Elsevier, Amsterdam, pp 549–618
57. Yoo MH (1986) ScriptaMetallurgica 20:915–920
58. Kear BH, Wilsdorf HGF (1962) Trans Metall Soc AIME 224:382–386
59. Copley SM, Kear BH (1967) Trans AIME 239:984–992
60. Murakumo T, Kobayashi T, Koizumi Y, Harada H (2004) Creep of Ni-base single-crystal superalloys with various gamma volume fraction. Acta Mater 52(12):3737–3744
61. Karunarante MSA, Reed RC (2003) Interdiffusion of platinum-group metals in nickel at elevated temperatures. Acta Mater 51(10):2905–2914
62. Reed RC, Karunarantne MSA (2000) Interdiffusion in the face-centered cubic Phase of Ni–Re, Ni–Ta and Ni–W systems between 900 °C and 1300 °C. Mater Sci Eng A 281(1–2):229–233
63. Walston WS, Cetel A, MacKay R, O'Hara K, Duhl D, Dreshfield R, Joint development of a fourth generation single crystal superalloy. TMS, Warrendale, PA, USA, pp 15–24
64. Tanaka R (2000) Research and development of ultra-high temperature materials in Japan. Mater High Temp 17(4):457–464
65. Shyam A, Torbet CJ, Jha SK, Larsen JM, Caton MJ, Szczepanski CJ, Pollock TM, Jones JW (2004) Development of ultrasonic fatigue for rapid, high temperature fatigue studies in turbine engine materials. TMS, Warrendale, PA, USA, pp 259–267
66. Miner RV, Gayada J, Maier RD (1982) Fatigue and creep fatigue deformation of several nickel-base superalloys at 650 °C. Metall Trans A 13A(10):1755–1765
67. Clavel M, Pineau A (1982) Fatigue behavior of two nickel-base alloys: Experimental results on low cycle fatigue, fatigue crack propagation and substructures. Mater Sci Eng 55(2):157–171
68. Chan KS, Hack JE, Leverant GR (1987) Fatigue crack growth in mar-m200 single crystals. Metall Trans 18A(4):581–591
69. Antolovich SD, Lerch B (1989) Cyclic deformation, fatigue and fatigue crack propagation in Ni-base alloys. In: Tien JK, Caulfield T (eds) Superalloys, supercomposites and superceramic. Academic Press, New York, USA, pp 363–412
70. Wright PK, Jain M, Cameron D (2004) High cycle fatigue in a single crystal superalloy: time dependence at elevated temperature. TMS, Warrendale, PA, pp 657–666
71. Crompton JS, Martin JW (1984) Crack growth in a single crystal superalloy at elevated temperature. Metall Trans A 15A:1711–1718
72. Larsen JM, Christodoulou (2004) Using materials prognosis to maximize the utilization of complex mechanical systems. J Met 56(3):15–28
73. Saunders N (1995) Phil Trans R Soc Lond A 351:543–561
74. Das N (2008) Unpublished work, DMRL, Hyderabad, India